SnailBot: A Continuously Dockable Modular Self-reconfigurable Robot Using Rocker-bogie Suspension

Da Zhao[1,2] and Tin Lun Lam[1,2,†]

***Abstract*— This paper proposes a novel modular self-assembling, self-reconfiguring robot with the 3D continuous dock called "SnailBot". SnailBot mainly consists of a spherical ferromagnetic shell and a six-wheel rocker chassis with embedded magnets. Unlike many other existing modular self-reconfigurable robots with fixed docking locations, SnailBot uses the 3D continuous dock to attach to its peers regardless of alignment. This freeform docking mechanism can greatly improve the efficiency of self-reconfiguration and reduce docking failures because there is nearly no constraint in the location of the connector. Compared with the existing freeform MSRR, SnailBot can form a more structurally stable connection to its peers without loss of connection efficiency. Owing to the excellent obstacle crossing ability of the rocker-bogie suspension, the robot can freely crawl on other modules in the form of a sliding sphere. Experiments demonstrate the basic actions of a single module and some applications of SnailBots, such as a manipulator.**

I. INTRODUCTION

Modular self-reconfigurable robots (MSRR) are generally considered more adaptive than fixed-morphology robots, due to their capability of rearranging the connectivity of their parts to form new morphologies that are better suitable for new tasks [1]–[6]. These robotic systems also have the potential to be self-healing by using redundant low-cost robotic modules to improve system robustness. These unique capabilities make them highly desirable in exploring unstructured or dynamic environments.

Although modular robots have the advantages of versatility and low cost, most of their connection mechanism is overly idealistic — they use fixed connection method to connect multiple modular robots, ignoring the practical issues, such as imperfect manufacturing. Previously, the connection mechanism of existing MSRR system mainly consists of retractable mechanical hook [4], [7], permanent magnet [1], [8], electromagnet [9] and self-soldering alloy [10], and all of them need dock-to-dock alignment. In large-scale self-assembly or self-reconfiguration, this reliance on a specific connector location can result in mission failure. To be specific, the possible reasons include accumulation of manufacturing deviation, low sensor precision, or deflection caused by gravity or external forces [2]. The misalignment caused by these inadequacies is very common in modular robot systems.

This work was supported by the National Natural Science Foundation of China (62073274), and the funding AC01202101103 from the Shenzhen Institute of Artificial Intelligence and Robotics for Society.

[1]School of Science and Engineering, The Chinese University of Hong Kong, Shenzhen, China.

[2]Shenzhen Institute of Artificial Intelligence and Robotics for Society.

[†]Corresponding author: Tin Lun Lam, e-mail: tllam@cuhk.edu.cn

(a) Snails (photo provided by [11]) (b) SnailBots

Fig. 1. SnailBot—MSRR system inspired by the anatomy of the snail.

In nature, a swarm of creatures can exhibit abilities that individuals do not possess. For example, A cluster of ants will assemble into a bridge to cross the gully or biological organisms achieve robust high-level behaviors by combining low-level components [12]. The way these creatures connect to each other is often not constrained to a lattice type and is very efficient. Inspired by biological structure, many researchers have developed modular robots that can form attachments without docking alignment, but many of them are limited to moving in a 2D plane [13]–[15]. To our knowledge, only two modular robots have demonstrated the ability of 3D continuous connection, which are FireAnt3D [16] and FreeBot [17], [18]. A given location on the dock surface of FireAnt3D only has a lifespan of about 50 attachment/disconnection cycles, and the cooling time takes 5 minutes, which is too long. FreeBot pioneered the freeform MSRR system, but the connection point between two FreeBots is a single point, which means that the overall structure is very unstable when two FreeBots are connected. Another limitation of FreeBot is that it only has two controllable DOFs. The inside trolley can drive the spherical shell to roll in two directions, but it cannot accurately control the rotation of the shell around its vertical axis.

Inspired by the anatomy of the land snail, this work presents a new reconfigurable robotic system – SnailBot. Similar to a snail having a shell and a strong muscular foot, SnailBot is mainly composed of a spherical ferromagnetic shell and a six-wheel rocker chassis with embedded magnets. The SnailBot can move between its peers by lifting its forearm. Different from many other existing modular self-reconfigurable robots with fixed docking locations, SnailBot uses the 3D continuous dock to attach to its peers regardless of alignment. This freeform docking mechanism can greatly improve the efficiency of self-reconfiguration and reduce docking failures because there is nearly no constraint in the location of the connector. Compared with the existing MSRR with a 3D continuous dock, SnailBot can form a more structurally stable connection to its peers without loss of

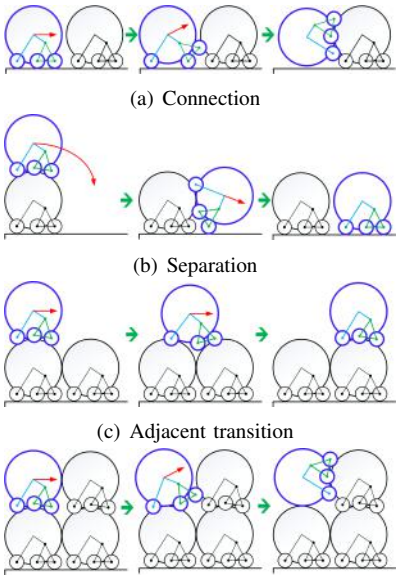

(a) Connection

(b) Separation

(c) Adjacent transition

(d) Nonadjacent transition

Fig. 2. Four motion primitives of a single modular robot.

connection efficiency. When the two modules are connected, they form a spherical joint with three controllable DOFs.

II. Geometric Parameter Optimization

A. Basic actions

In order for modular robots to realize self-assembly and self-reconfiguration, a single modular robot needs to be able to autonomously attach to or detach from its peers. The ability to move over other modules is also indispensable. [19] has given us a brief analysis of the basic actions of the freeform modular robot self-reconfiguration. Similarly, we define four basic actions for a single robot, including *connection*, *separation*, *adjacent transition* and *nonadjacent transition*, as shown in Fig. 2.

The action *connection* and *separation* enable the modular robot group to self-assemble and these two motion primitives only occur when the robot is about to touch or leave the ground. However, *adjacent transition* and *nonadjacent transition* are usually carried out in 3D space, which means that the moving robot can have a variety of poses. For simplicity's sake, in Fig. 2(c) and Fig. 2(d), we only draw one of the cases, respectively.

B. Geometric Constraint

In order to successfully perform these basic actions, there are many constraints on the size of the modular robot. In this paper, we address this problem using an optimization-based method. Before formulating the geometric constraints of the robot as an optimization problem, we need to use symbols to define the various size parameters of the robot, as shown in Fig. 3. After some simple analysis, we know that this robot can be defined by at least 7 dimension parameters, which are $R, r, \theta_2, \theta_3, l_2, l_4, l_6$. These basic sizes are shown in red in Fig. 3. Other dimensions shown in blue all can be calculated from these 7 red ones, such as

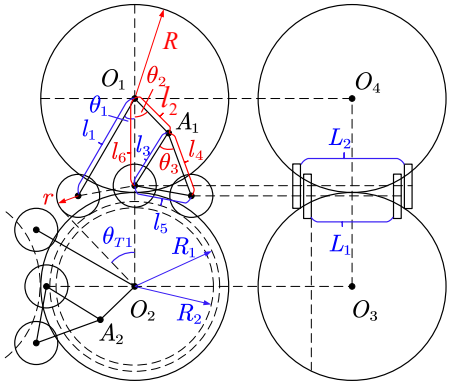

Fig. 3. Symbolic representation of dimension parameters

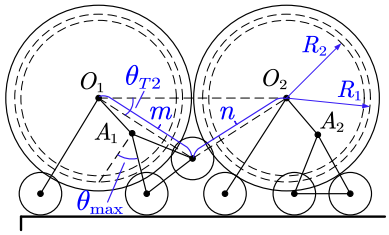

Fig. 4. The robot tries to attach to its peers

$$L_2 = 2\sqrt{R^2 - R_2^2} = 2\sqrt{R^2 - (2R - l_6 - r)^2} \tag{1}$$

We hope that a robot can be connected to 5 robots simultaneously, so the coverage area of six wheels had to be limited. In Fig. 3, the angle θ_{T1} should be less than $\pi/4$, then we have

$$\theta_{T1} = \frac{r}{R_1 + r} + \arcsin\frac{l_1 \sin\theta_1}{R_1 + r} < \frac{\pi}{4} \tag{2}$$

The geometric parameter representation of the connection process is shown in Fig. 4. When the robot performs the *connection* action and lifts the rocker arm to its maximum, the front wheels need to touch the shell of the passively connected robot to obtain the upward friction force. Before two robots' shells touch, the distance between the front wheel and the center of the connected robot shell needs to be less than the sum of R_1 and r, then we have

$$n = \sqrt{m^2 + 4R^2 - 4Rm\cos(\theta_{T2})} < R_1 + r \tag{3}$$

The same happens when the robot performs a *nonadjacent transition* action, as shown in Fig. 5. Before two shells collide, the front wheel of the mobile robot needs to touch the shell of the front module to provide upward lift. We obtain

$$n' = \sqrt{m^2 + 4R^2 - 4Rm\cos(\theta_{T3})} < R_1 + r \tag{4}$$

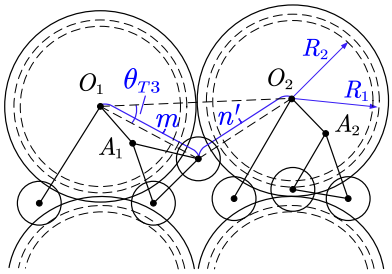

Fig. 5. The robot prepare to execute the *nonadjacent transition* action.

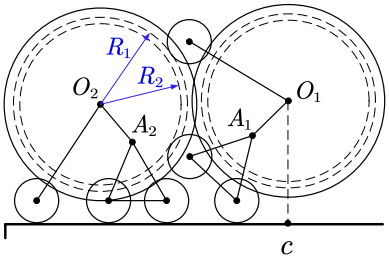

Fig. 6. The robot tries to separate from its peers.

In Fig. 6, when the Snailbot tries to detach from another one, its front wheels need to touch the ground to provide a frictional force for forward drive. Then we have

$$O_1c > R \tag{5}$$

C. Nonlinear Optimization

The size optimization problem of this modular robot can be formulated as a nonlinear optimization problem. Eq. (2), Eq. (3), Eq. (4) and Eq. (5) represent nonlinear constraints. In order to make the moving robot have the better passing ability when it executes *adjacent transition*, the sum of the distance between the front and rear wheels and the wheel diameter of the base robot should be as small as possible. Therefore, this optimization problem can be formulated as

$$\min \ f = l_1 \sin\theta_1 + r$$

$$s.t. \begin{cases} \frac{r}{R_1+r} + \arcsin\frac{l_1\sin\theta_1}{R_1+r} < \frac{\pi}{4} \\ n = \sqrt{m^2+4R^2-4Rm\cos(\theta_{T2})} < R+r \\ n' = \sqrt{m^2+4R^2-4mR\cos(\theta_{T3})} < R_1+r \\ l_5 - 2r \geq 0 \\ O_1c_2 > R \\ for\ x_i, (i=1,2\cdots 6) : lb_i \leq x_i \leq ub_i. \end{cases}$$

where $x_i, (i = 1, 2\cdots 6)$ represents the six basic sizes $r, \theta_2, \theta_3, l_2, l_4, l_6$.

With the help of some nonlinear optimization solvers, we can get $r^* = 0.26R$, $l_2^* = 0.71R$, $l_4^* = 0.82R$, $l_6^* = 1.09R$, $\theta_2^* = 55$deg, $\theta_3^* = 50$deg. Once the shell radius is given, other geometric parameters can be determined. The shell radius of the SnailBot is 120mm.

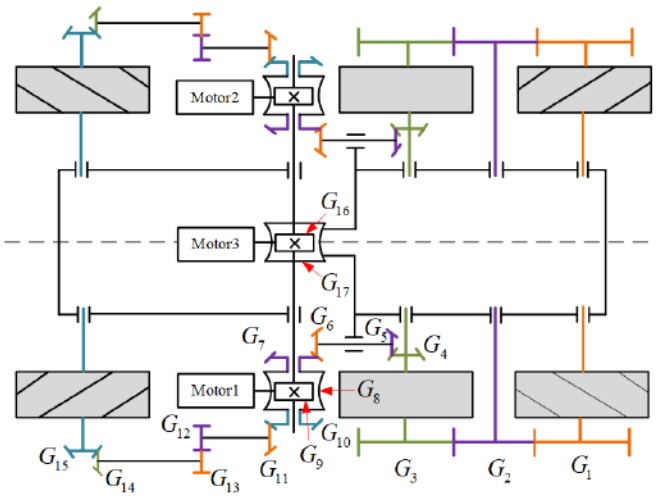

Fig. 7. Mechanical schematic of the transmission system.

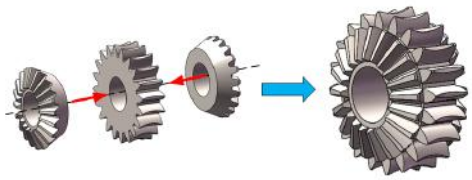

Fig. 8. Formation process of a bevel-worm gear. This special shaped gear is made by metal printing.

III. Driving System

There are many challenges in the design of the drive system of a six-wheel modular robot because of strict constraints in its weight and size. Most existing six-wheel rocker-bogie chassis (such as lunar rover) are driven by six motors, and the front and rear four wheels have separate steering motors. If Snailbot's drive system is also designed in a traditional way, it will have at least 11 motors, which will greatly increase the weight of the robot. In this section, we will show the innovative design of the robot drive system, including a parallel-type coaxial differential transmission system and a hybrid-type six-wheel chassis.

A. Parallel-type Coaxial Differential Transmission System

The number of driving motors for Snailbot is three: two drive wheels and one drives forearm. Each motor that powers the wheels can drive three wheels on one side. The explosion view of the transmission system and its mechanical schematic is shown in Fig. 7 and Fig. 9, respectively. The whole transmission system is designed in parallel, and the transmission center is a bevel-worm gear. The two sides of the bevel-worm gear are bevel gears, and the middle is the worm gear. The motor provides power to drive the middle worm gear, and the bevel gears on both sides transmit power to the front four wheels and the rear wheels, respectively. In Fig. 8, we show the formation process of a bevel-worm gear. This compact design can greatly reduce the mechanical design complexity of the transmission center.

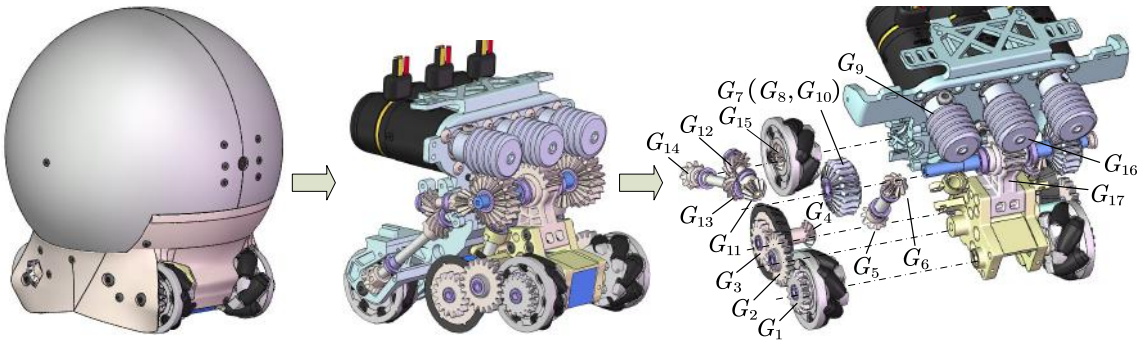

Fig. 9. CAD model of the Snailbot and its explosion view.

When Snailbot is attached to another module, its arm lifting action is especially important for the completion of *separation* and *transition*. To make it easier to lift the forearm, our driveline includes a coaxial differential system. In addition to the side motors that can drive six wheels, the middle arm motor can also drive the first four wheels. When lifting the rocker arm, this design transforms the sliding friction between the middle wheel and the shell into rolling friction, which can greatly reduce the torque required to lift the arm and reduce wheel wear.

The angular velocity of the rocker arm and rear wheel can be calculated by the following formula

$$\omega_{rocker} = \frac{z_{16}}{z_{17}}\omega_{mm} \tag{6}$$

$$\omega_{rw} = \frac{z_8}{z_{15}}\omega_{sm} \tag{7}$$

where ω_{mm} and ω_{sm} represent the angular velocity of the middle motor and the side motor, respectively. z_i $(i = 1, 2, \cdots, 17)$ denotes the number of teeth of gear i.

The angular velocity of the front four wheels is determined jointly by the middle motor and the side motor, which can be expressed as

$$\omega_{fw} = \frac{z_7}{z_4}\omega_{rocker} + \frac{z_8}{z_4}\omega_{sm} = \frac{z_7}{z_4}\frac{z_{16}}{z_{17}}\omega_{mm} + \frac{z_8}{z_4}\omega_{sm} \tag{8}$$

Fig. 10 illustrates the state of Snailbot when its rocker is raised to the maximum angle. The green arc represents the length of the middle wheel traveling across the shell, and the red arc represents the rotation of the middle wheel due to the rotation of the rocker. They need to be as equal as possible, so the gear ratio between gear 7 and gear 4 can be calculated as

$$\frac{z_7}{z_4} = \frac{R_2\theta_{T4}}{r\theta_{max}} \tag{9}$$

Based on the parameter optimization results in Section II, the final result of Eq. (9) is approximately 2. Taking into account the need for consistent wheel speed and steering on each side, as well as the space limitation of the robot, the number of teeth, modulus, and shaft angle of all gears were finally determined, as shown in Table I.

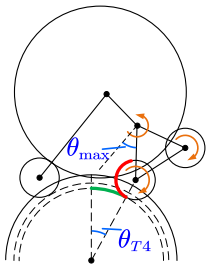

Fig. 10. An illustration of lifting the arm when Snailbot is attached to another module.

TABLE I

PARAMETERS OF GEARS

Gear Code	Gear Type	No. of Teeth/Threads	Shaft Angle
G1	Spur gear	16	-
G2	Spur gear	20	-
G3	Spur gear	16	-
G4	Bevel gear	10	π/2
G5	Bevel gear	10	
G6	Bevel gear	10	π/2
G7	Bevel gear	20	
G8	Worm gear	20	-
G9	Worm	1	-
G10	Bevel gear	20	π/2
G11	Bevel gear	10	
G12	Spiral gear	10	π/6
G13	Spiral gear	10	
G14	Spiral gear	10	π/2
G15	Spiral gear	10	
G16	Worm	1	-
G17	Worm gear	20	-

* The modulus of all the gears is 1.

B. Hybrid Type Six Wheel Chassis

When two robots are connected, the actively connected one is subjected to a magnetic force equivalent to several times the gravity. If ordinary wheels are still used in the front and back of the chassis, the robot will experience great resistance when turning. In this case, we propose a hybrid six-wheel chassis design – the front and rear four wheels are mecanum wheels, and the middle wheels are ordinary wheels, as shown in Fig. 11.

From the bottom up, the rollers of the four mecanum wheels with the proposed layout are arranged in an X-

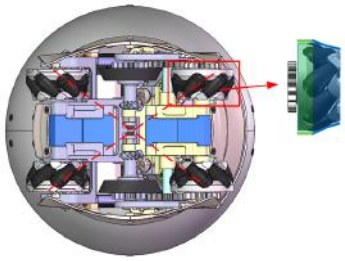

Fig. 11. A hybrid type six wheel chassis, including four mecanum wheels and two ordinary wheels. The wheels are designed to accommodate both flat (green area) and spherical (blue area) surfaces.

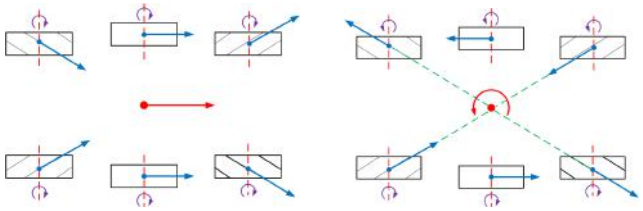

(a) Go Straight (b) Turn

Fig. 12. Force analysis of six wheels when SnailBot moves. The blue arrow represents the direction of the force on the wheel

shape, while those of the traditional omnidirectional moving platform are arranged in an O-shape. The advantage of this design is that when the six wheels are driven forward or backward, the four mecanum wheels on the periphery can provide the driving force. When the robot turns, they only act as guide wheels. The detailed force analysis is shown in Fig. 12.

IV. The 3D Continuous Dock

The 3D continuous docking mechanism is one of the most important mechanisms of freeform MSRR. FreeBot [17] utilize a permanent magnet and ferromagnetic spherical shell to realize fast 3D continuous docking. Similar to FreeBot, Snailbot has magnets embedded in the middle of the chassis and relies on them for attaching. Due to the mobility of the rocker-bogie suspension, the magnets of SnailBot can be roughly divided into two parts: the front part is fixed to the rocker arm, and the other part is installed between the two rear wheels, as shown in Fig. 13.

The size, layout of the magnets, as well as the distance between the magnet and the spherical shell determine the self-reconfigurable ability of SnailBot. In Fig. 13, the force analysis of SnailBot when connecting or separating from other modules is illustrated. Based on the force analysis, we know that the key to complete the two actions is that there is enough friction between the robot's wheels and the ground or the sphere. The friction force F_{C1} and F_{C2} on the rear wheel can increase the pressure between the front wheel and the contact surface, thus increasing the friction force on the front wheels. Specifically, F_{A1} and F_{A2} in Fig. 13 need to be able to rotate the module itself. The forces applied to the SnaiBot during the $adjacent\ transition$ action are similar to the $separation$ action.

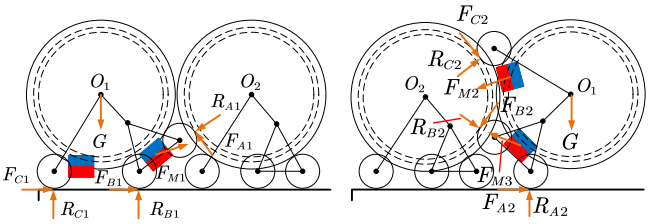

Fig. 13. Force analysis when connecting / separating.

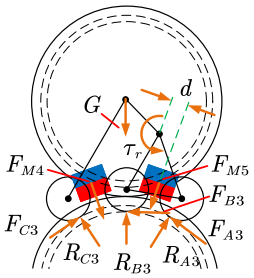

Fig. 14. Force analysis when lifting the rocker.

Fig. 14 illustrates the force analysis when the SnailBot is lifting the rocker. If the front and rear magnets have the same magnetic force or the back magnet is less powerful than the front, the back of the SnailBot may tilt up. Therefore, the rear of the robot must be subjected to more magnetic force than the front. Owing to the transmission system mentioned in Section III, there is little sliding friction between the middle wheels and the shell when the robot lifts the rocker. F_{B3} is therefore very small and negligible. The main resistance of raising the rocker comes from the magnetic force between the front magnet and the spherical shell. The torque of the middle motor should meet the following requirement:

$$\tau_{mm} > \frac{z_{16}}{z_{17}} \frac{F_{M5} d}{\eta} \tag{10}$$

where η denotes the transmission efficiency between worm 16 and worm gear 17.

The arrangement of multiple magnets also has different forms, such as alternating polarity, same polarity oriented along the largest dimension or same polarity oriented along the smallest dimension [20]. Here, we adopt four magnets which are commercially available neodymium cubes of 15x15x15mm with a strength of N52. The magnets are arranged with alternating polarity and this arrangement can make full use of the space at the bottom of the robot, as shown in the left of Fig. 15. The rear magnet is 0.5mm closer to the shell than the front magnet, which makes the magnetic force between the rear magnet and the spherical shell stronger, so as to ensure that the rear of the robot will not tilt when raising the rocker. Take the height of the rear magnets as the reference, the variation of magnetic force with the distance between force magnets and the shell is shown in Fig. 15. At present, the height of the rear magnet from the shell is 1.75mm, and the normal force of these magnets is 86.7N, which is about equal to the mass of eight modules.

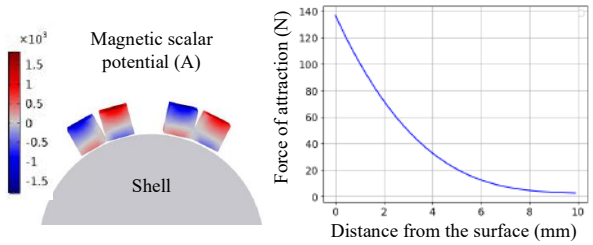

Fig. 15. Magnetic force vs. distance between magnets and the shell.

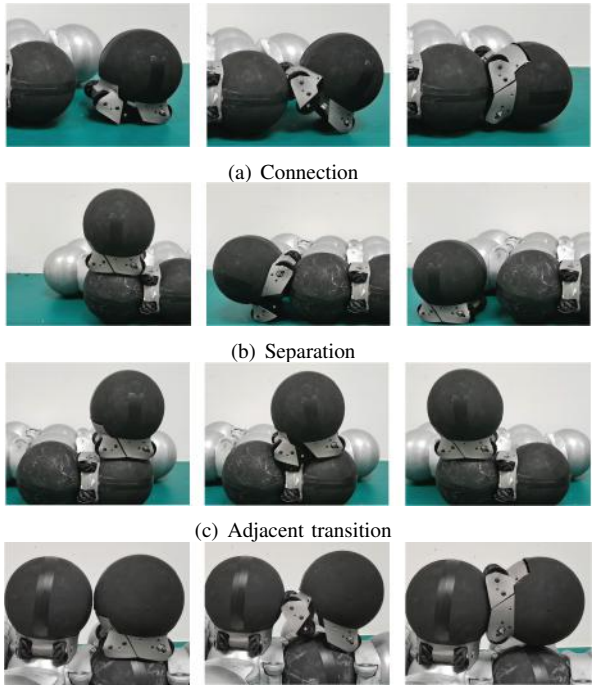

(a) Connection

(b) Separation

(c) Adjacent transition

(d) Nonadjacent transition

Fig. 16. Four basic actions of a single modular robot.

V. Experiments

Experiments were performed to demonstrate the locomotion ability of the SnaiBot, including various basic actions of a single robot and cooperative movements of multiple modules. All robots are controlled by remote control.

A. Basic actions

Fig. 16 illustrate the four basic actions of a single modular robot. The rocker chassis presents super-strong obstacle crossing ability, so a single robot module can connect to, separate from other modules, or move over multiple robots. These four basic actions enable the multi-SnailBot system to self-reconfiguration and self-assembly.

B. Manipulator

Multiple SnailBots can form a robot arm and carry other items, as shown in Fig. 17. When two robot modules are connected, the joint is equivalent to a spherical joint with nonholonomic constraints (due to the differential car). The two modules can grip other objects like claws and rely on the movement of the modules below to carry objects.

(a) (b) (c)

Fig. 17. Multiple SnailBots form a robotic arm to carry the box.

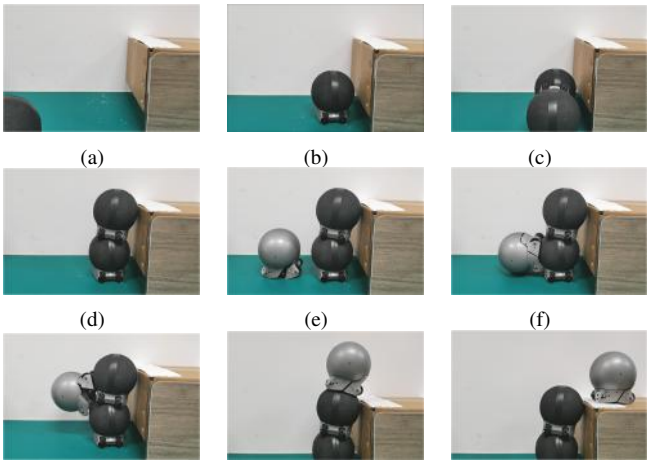

(a) (b) (c)

(d) (e) (f)

(g) (h) (i)

Fig. 18. Three SnailBots collaborate to climb the obstacle.

C. Three SnailBots Collaborate to climb the obstacle

Cooperating to complete some tasks that a single module cannot complete is a major feature of modular robots. As shown in Fig. 18, three SnailBot modules can work together to surmount an obstacle higher than a single module. Multiple modules can stack on each other until they are above the obstacle. Subsequent modules can climb to their destination using a previously constructed ”ladder”. This vertical climbing capability is very important for the self-reconfiguration of multiple robots. With this ability, SnailBots can form a variety of 3D structures.

VI. Conclusions and Future Work

In this paper, we propose a biologically inspired modular self-reconfiguring robot called ”SnailBot”, which is mainly composed of a spherical ferromagnetic shell and a six-wheel rocker chassis with embedded magnets. SnailBot uses the 3D continuous dock to attach to its peers regardless of alignment. This freeform docking mechanism can greatly improve the efficiency of self-reconfiguration and reduce docking failures because there is nearly no constraint in the location of the connector. The magnet-based docking mechanism can make the robot connect more stably without losing efficiency. Several experiments have also demonstrated the potential of SnailBots to build freeform MSRR systems.

In the future, we will advance the automation of the SnailBot system, including building a perception system for each module and studying self-reconfiguration algorithms. SnailBots will also be tested in more complex environments.

REFERENCES

[1] J. Davey, N. Kwok, and M. Yim, "Emulating self-reconfigurable robots-design of the smores system," in *2012 IEEE/RSJ international conference on intelligent robots and systems*. IEEE, 2012, pp. 4464–4469.

[2] A. Spröwitz, R. Moeckel, M. Vespignani, S. Bonardi, and A. J. Ijspeert, "Roombots: A hardware perspective on 3d self-reconfiguration and locomotion with a homogeneous modular robot," *Robotics and Autonomous Systems*, vol. 62, no. 7, pp. 1016–1033, 2014.

[3] S. Murata, E. Yoshida, A. Kamimura, H. Kurokawa, K. Tomita, and S. Kokaji, "M-tran: Self-reconfigurable modular robotic system," *IEEE/ASME transactions on mechatronics*, vol. 7, no. 4, pp. 431–441, 2002.

[4] H. Wei, Y. Chen, J. Tan, and T. Wang, "Sambot: A self-assembly modular robot system," *IEEE/ASME Transactions on Mechatronics*, vol. 16, no. 4, pp. 745–757, 2010.

[5] P. Levi, E. Meister, A. C. van Rossum, T. Krajnik, V. Vonásek, P. Stepan, W. Liu, and F. Caparrelli, "A cognitive architecture for modular and self-reconfigurable robots," in *2014 IEEE International Systems Conference Proceedings*. IEEE, 2014, pp. 465–472.

[6] U. A. Fiaz and J. S. Shamma, "Usbot: A modular robotic testbed for programmable self-assembly," *IFAC-PapersOnLine*, vol. 52, no. 15, pp. 121–126, 2019.

[7] C. H. Belke and J. Paik, "Mori: a modular origami robot," *IEEE/ASME Transactions on Mechatronics*, vol. 22, no. 5, pp. 2153–2164, 2017.

[8] J. W. Romanishin, K. Gilpin, S. Claici, and D. Rus, "3d m-blocks: Self-reconfiguring robots capable of locomotion via pivoting in three dimensions," in *2015 IEEE International Conference on Robotics and Automation (ICRA)*. IEEE, 2015, pp. 1925–1932.

[9] T. Tosun, J. Davey, C. Liu, and M. Yim, "Design and characterization of the ep-face connector," in *2016 IEEE/RSJ International Conference on Intelligent Robots and Systems (IROS)*. IEEE, 2016, pp. 45–51.

[10] J. Neubert, A. Rost, and H. Lipson, "Self-soldering connectors for modular robots," *IEEE Transactions on Robotics*, vol. 30, no. 6, pp. 1344–1357, 2014.

[11] A. A. Amer, "Palestinians rediscover vast appetite for snails," Website, 2020, https://www.al-monitor.com/originals/2020/03/snails-a-traditional-dish-in-some-palestinian-villages.html.

[12] A. Haeger, K. Wolf, M. M. Zegers, and P. Friedl, "Collective cell migration: guidance principles and hierarchies," *Trends in cell biology*, vol. 25, no. 9, pp. 556–566, 2015.

[13] S. Li, R. Batra, D. Brown, H.-D. Chang, N. Ranganathan, C. Hoberman, D. Rus, and H. Lipson, "Particle robotics based on statistical mechanics of loosely coupled components," *Nature*, vol. 567, no. 7748, pp. 361–365, 2019.

[14] M. Shimizu and A. Ishiguro, "An amoeboid modular robot that exhibits real-time adaptive reconfiguration," in *2009 IEEE/RSJ International Conference on Intelligent Robots and Systems*. IEEE, 2009, pp. 1496–1501.

[15] M. Malley, B. Haghighat, L. Houe, and R. Nagpal, "Eciton robotica: Design and algorithms for an adaptive self-assembling soft robot collective," in *2020 IEEE International Conference on Robotics and Automation (ICRA)*. IEEE, 2020, pp. 4565–4571.

[16] P. Swissler and M. Rubenstein, "Fireant3d: a 3d self-climbing robot towards non-latticed robotic self-assembly," in *2020 IEEE/RSJ International Conference on Intelligent Robots and Systems (IROS)*. IEEE, 2020, pp. 3340–3347.

[17] G. Liang, H. Luo, M. Li, H. Qian, and T. L. Lam, "Freebot: A freeform modular self-reconfigurable robot with arbitrary connection point-design and implementation," in *2020 IEEE/RSJ International Conference on Intelligent Robots and Systems (IROS)*. IEEE, 2020, pp. 6506–6513.

[18] T. L. Lam and G. Liang, "Self-reconfigurable robot module and self-reconfigurable robot," Jul. 8 2021, uS Patent App. 17/134,066.

[19] H. Luo, M. Li, G. Liang, H. Qian, and T. L. Lam, "An obstacle-crossing strategy based on the fast self-reconfiguration for modular sphere robots," in *2020 IEEE/RSJ International Conference on Intelligent Robots and Systems (IROS)*. IEEE, 2020, pp. 3296–3303.

[20] A. San-Millan, "Design of a teleoperated wall climbing robot for oil tank inspection," in *2015 23rd Mediterranean Conference on Control and Automation (MED)*. IEEE, 2015, pp. 255–261.